J Mater Sci (2011) 46:3846–3854
DOI 10.1007/s10853-011-5301-6

Solubility and formation of ternary Widmanstätten precipitates in PbTe in the pseudo-binary PbTe–Bi_2Te_3 system

Teruyuki Ikeda · Marcus B. Toussaint · Kristin Bergum · Shiho Iwanaga · G. Jeffrey Snyder

Received: 15 December 2010 / Accepted: 17 January 2011 / Published online: 1 February 2011

Abstract A unidirectional solidification experiment by Bridgman method has been performed for the $Pb_{14}Bi_{28.8}Te_{57.2}$ composition, which lies on the pseudo-binary PbTe–Bi_2Te_3 system, resulting in the formation of Widmanstätten precipitates of a ternary compound, most likely with the structure of $PbBi_2Te_4$ in the PbTe matrix. The formation of the precipitates is caused by the decrease of bismuth solubility in the PbTe phase with decreasing temperature. The PbTe-rich part of the PbTe–Bi_2Te_3 phase diagram was investigated from the compositional variations in the unidirectionally solidified sample and the diffusion couples. This proved that the solubility decreases with decreasing temperature: 15.6 ± 0.9 (583 °C) to $6.2^{+2.1}_{-1.7}$ (450 °C) at.% Bi. The orientation relationship between the matrix and precipitates has been examined by electron backscatter diffraction technique; precipitation occurs on {111} habit planes in PbTe with orientation relationship $(0001)_{precipitate}//\{111\}_{PbTe}$ and $<11\bar{2}0>_{precipitate}//<110>_{PbTe}$. The thermoelectric properties in PbTe with Widmanstätten precipitates as examined by the scanning Seebeck probe method is $-46 \pm 2\ \mu VK^{-1}$.

T. Ikeda
PRESTO, Japan Science and Technology Agency, 4-1-8 Honcho, Kawaguchi, Saitama 332-0012, Japan

T. Ikeda (✉) · M. B. Toussaint · K. Bergum · S. Iwanaga · G. Jeffrey Snyder
Materials Science, California Institute of Technology, 1200 California Blvd., Pasadena, CA 91125, USA
e-mail: tikeda@caltech.edu

Introduction

In nanostructured materials, phonons are scattered at interfaces [1], which can reduce the lattice component of the thermal conductivity [2]. This reduced thermal conductivity can lead to thermoelectric materials with a high thermoelectric figure of merit, zT, defined as $S^2\sigma/\kappa$, where S is the Seebeck coefficient, σ the electrical conductivity, and κ the thermal conductivity. Substantial zT has been observed in structures with small nanoparticles [3] as well as larger precipitates in PbTe–Ag_2Te [4].

Solid-state phase transformation is an effective route to introduce nanostructure in bulk thermoelectric materials [5]; e.g. in the PbTe–Sb_2Te_3 system, nanolamellar structure is formed by a eutectoid reaction [6, 7] and κ_{lat} has been found to decrease as the inter-lamellar spacing decreases [8]. Plate-shaped Sb_2Te_3 precipitates in PbTe [9] and the size scale of the precipitation structure has been controlled [10, 11]. Plate precipitates, so called Widmanstätten plates, have larger interface area per unit volume than, for e.g., spherical particles compared for the same volume fraction and number density because of their shape and hence could be more effective in reducing the lattice thermal conductivity. However, such an impact of nanostructuring on the lattice thermal conductivities has not been systematically studied by changing particle size or morphology.

While nanostructure formation in the PbTe–Bi_2Te_3 system, where both PbTe and Bi_2Te_3 show good thermoelectric properties, has not been reported so far, similar solid-state reactions to the PbTe–Sb_2Te_3 system may be expected because of the chemical kinship between Bi and Sb. In phonon scattering at interfaces, the mass contrast of the phases consisting of the interfaces and the interface structure are important key parameters [12]. Comparisons

of different precipitates in PbTe matrices would be a helpful tool in understanding the reduction in κ_{lat} and enhancement of zT. The thermoelectric properties of compounds in this system have been studied within the solid solution PbTe up to 1.94 at.% Bi [13] and 0.84 at.% Bi [14]. While several research groups have investigated the phase diagram of the pseudo-binary PbTe–Bi_2Te_3 system [15, 16], the solubility in the PbTe phase in equilibrium with a solid phase has been measured only at 500 °C [16, 17] as shown in Fig. 1. Unidirectional solidification by Bridgman method is a powerful tool to obtain qualitative information on phase diagrams such as phase equilibria, temperature dependence of solubility, etc. In this article, a unidirectional solidification experiment by the Bridgman method has been conducted to investigate the PbTe-rich region of the phase diagram in the pseudo-binary PbTe–Bi_2Te_3 system and to show the formation of Widmanstätten precipitates, which could be effective in reduction of the lattice thermal conductivity in thermoelectric PbTe. The structural features of the precipitates such as composition and orientation relationship with the matrix PbTe are discussed. The solubility range in the PbTe phase is also determined as a function of temperature by diffusion couple experiments to prove that the precipitates form due to the reduction of solubility range of PbTe phase with decreasing temperature. The knowledge on the solubility range is also quite important in order to understand transport properties since point defect structure of the matrix phase in the precipitation structure is closely connected to the composition of the matrix phase.

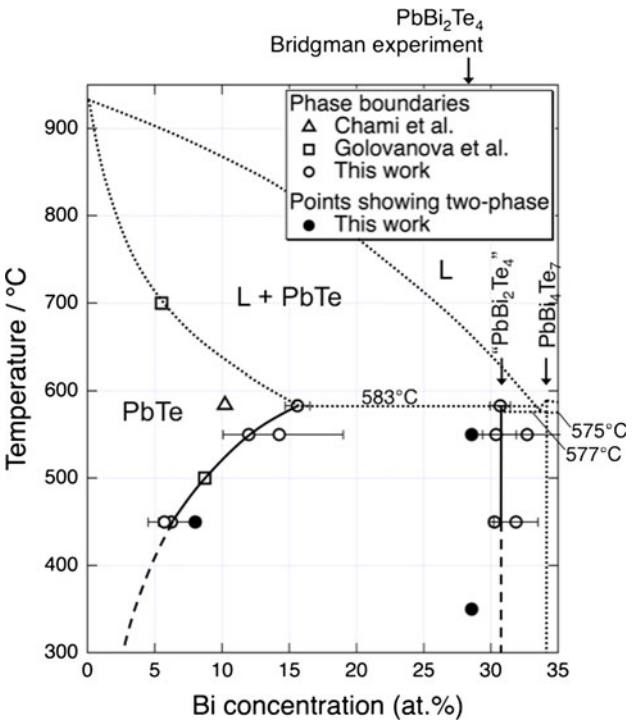

Fig. 1 PbTe-rich part of the equilibrium phase diagram of the pseudo-binary PbTe–Bi_2Te_3 system based on the previous report [18] (*dotted lines*) and this work (*solid and dashed lines*). The diagram also includes the existence range of PbTe phase reported by Chami et al. [16], Golovanova et al. [17]. The data point plotted at the peritectic temperature 583 °C [16] is the maximum solubility in the PbTe phase and the composition of the phase crystallized next to (*above*) the PbTe phase in the unidirectionally solidified sample by Bridgman method. The data points plotted at 450 and 550 °C were determined using PbTe/Bi_2Te_3 diffusion couples. The *top arrow* indicates the composition at which the unidirectional solidification experiment was carried out in this study and which is close to the nominal composition of $PbBi_2Te_4$. The *solid circles* show the points where isothermal annealing experiments were carried out and the samples are composed of two phases. Further studies are needed for the Bi_2Te_3 rich-side boundary of "$PbBi_2Te_4$"

Experimental

Bridgman method

Stoichiometric quantities of Pb, Bi, and Te granules (8.2 g in total) were loaded into a fused silica ampoule with 6 mm inner diameter and then sealed under argon gas of approximately 3.4×10^4 Pa to obtain an alloy with overall composition of $Pb_{14}Bi_{28.8}Te_{57.2}$, which lies on the pseudo-binary line between PbTe and Bi_2Te_3. To avoid contact between the fused quartz and sample, the inside of the fused quartz tube was coated with carbon by imperfect combustion of acetone. The sample was then inductively melted for approximately 5 min and subsequently cooled in air. Unidirectional solidification was performed using a Bridgman-type furnace; the ampoules were moved downwards with a velocity of 0.37 mm h^{-1}. The furnace temperature was set to 800 °C. The temperature gradient was ~27 °C mm^{-1} at temperatures close to the liquidus temperature, ~650 °C, reported in the PbTe–Bi_2Te_3 phase diagram [18]. A sample thus obtained (hereafter, "as solidified" state) was cut in half longitudinally for microstructural observations.

The inner cross sections were exposed by cutting with a diamond saw and polished with a series of SiC papers up to #800, then polished with a series of Al_2O_3 powder (3–0.3 μm), and finally with colloidal silica (0.05 μm). The microstructure was observed using a field emission-scanning electron microscope (FE-SEM, Carl Zeiss LEO 1550 VP) equipped with a backscattered electron detector. The accelerating voltage was 20 kV. The chemical composition was measured as a function of the distance from the bottom end of the sample using a wavelength dispersive X-ray spectrometer (WDS, JXA-8200, JEOL Ltd.) with Bi and PbTe samples as standards for ZAF conversion [19] from intensities of Pb M_α, Bi M_α and Te L_α to concentrations. The accelerating voltage was 15 kV. To determine the

average composition of hetero-phase microstructure, the probe diameter was set to 25 μm. The crystallographic orientations in the microstructures were determined using the electron backscatter diffraction technique (EBSD; HKL Technology, Inc.). The operating voltage of the electron beam for EBSD was 20 kV. The surface of the samples was inclined at 70° to the vertical direction with respect to the electron beam. Electron backscatter patterns were analyzed using a commercial software package Channel 5^{TM} (HKL Technology, Inc.).

Determination of solubility range of PbTe by diffusion couples

The solubility range in PbTe phase in the PbTe–Bi_2Te_3 system was examined at two temperatures, 450 and 550 °C, using PbTe/Bi_2Te_3 diffusion couples. PbTe and Bi_2Te_3 were synthesized by induction heating under argon atmosphere followed by annealing at 585 °C for 24 h and at 400 °C for 24 h, respectively, for homogenization. The experimental set up for making diffusion couples is the same as described elsewhere [20]. The polished planes of Bi_2Te_3 and PbTe samples were brought into contact using a stainless steel clamp. The clamp holding a couple of Bi_2Te_3 and PbTe samples was wrapped in Ti and Ta foil and was sealed in a quartz tube with 30 kPa Ar. The couple was heat treated at 520 °C for 30 min for diffusion bonding. After the bonding, the diffusion couple was cut into four pieces perpendicularly to the bonded interface. Each piece was annealed at 550 °C (15 or 64 h) or 450 °C (9 or 24 days) to determine the phase boundaries at these temperatures. The concentration profiles were measured by WDS.

Isothermal heat treatments

A sample with $Pb_{40}Bi_8Te_{52}$ composition (8 at.% Bi), which also lies on the pseudo-binary PbTe–Bi_2Te_3 system, was synthesized, annealed at 585 °C for 7 days for homogenization, and annealed at 450 °C for 38 h to confirm the phase boundary determined by the diffusion couple experiments and reproduce the Widmanstätten precipitates. In order to check the phase stability of a ternary intermediate phase at two relevant temperatures (350 and 550 °C) in the PbTe–Bi_2Te_3 system, a sample with $Pb_{14.3}Bi_{28.6}Te_{57.1}$ composition corresponding to "$PbBi_2Te_4$" was annealed at 550 °C for 7 days and further annealed at 350 °C for 10 days. The annealing compositions (temperature and composition) for both the isothermal annealing experiments are indicated in Fig. 1. After the heat treatments, the microstructure was observed by FE-SEM. Powder X-ray diffraction experiments (XRD, Phillips X-Pert Pro diffractometer, Cu K_α radiation) have been carried out on this sample to identify phases.

Measurement of Seebeck coefficient

The Seebeck coefficient was measured near room temperature as a function of the distance from the bottom edge. After the surface of the sample was polished finally with 1 μm Al_2O_3 powder, the sample was mounted on a temperature-controlled copper plate to provide the uniform heat throughout the sample. In general, the Seebeck coefficient measurement requires the sample to have a temperature difference at two locations within a sample, which causes the Seebeck voltage to be generated. The temperature difference ΔT and the voltage difference ΔV between these locations are measured to calculate the Seebeck coefficient using the equation $\Delta V = S\Delta T$. In this particular measurement, the temperature difference was created between a thermocouple with a small thermal mass located at a corner of the sample, and a cold scan probe with a large thermal mass, which locally draws heat from the sample surface to create the local ΔT. The procedure is similar to that described in [21].

Results and discussion

Formation of Widmanstätten precipitates in PbTe by unidirectional solidification

The composition in the sample which was unidirectionally solidified using the Bridgman method was measured as a function of the distance from the bottom end. Since the beam size in the chemical composition measurement by WDS, 25 μm, is much larger than the size of the microstructure the measured composition reflects the average composition in the region. The compositions plotted in the ternary phase diagram of the Pb–Bi–Te system in Fig. 2a are found to lie almost on the pseudo-binary line for the PbTe–Bi_2Te_3 system. Figure 2b shows the variation of composition with the position. At the lowest part (up to 10 mm), a PbTe solid solution base compound is formed. This is consistent with the phase diagram (Fig. 1), where the primary solidification is predicted to occur with the PbTe phase. The Bi concentration c_{Bi} continues to increase in the PbTe solid solution base region as the unidirectional solidification proceeds. This is again expected from the phase diagram because with an increase in the volume of PbTe crystal, the liquid composition should shift to the PbTe deficient direction in the pseudo-binary system and so the composition of PbTe phase which is in equilibrium with the liquid should also shift to the compositions containing more Bi. Then, when the liquid composition eventually reaches the peritectic composition ($c_{Bi} \sim 33$ at.% according to [18]), an intermediate phase begins to crystallize. The jump of composition in the concentration

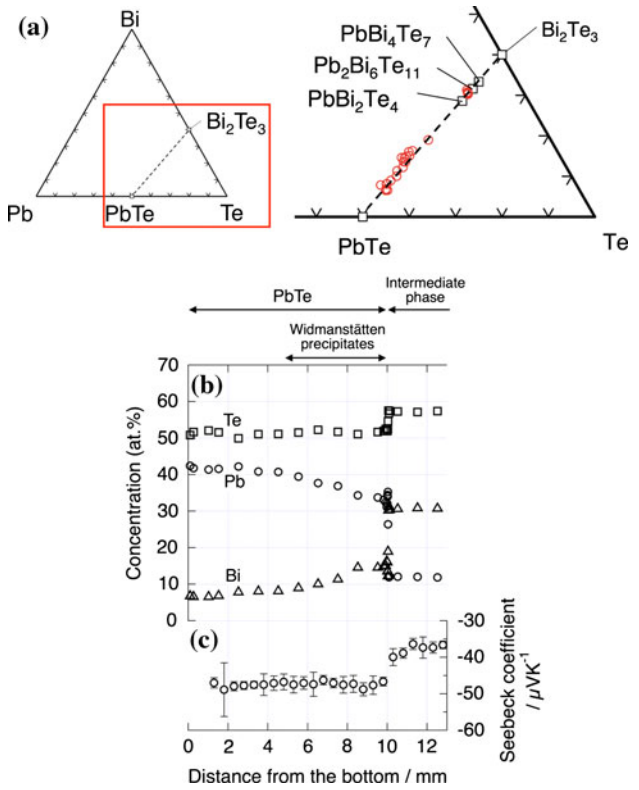

Fig. 2 Compositions in the PbTe-rich region in $Pb_{14}Bi_{28.8}Te_{57.2}$ unidirectionally solidified by Bridgman method. The partial ternary diagram in the Pb–Te–Bi system (**a**) is for the region indicated by red in the ternary phase diagram on the left. The compositions and Seebeck coefficient are plotted as functions of the distance from the bottom end of the sample in **b** and **c**, respectively. The *error bars* for Seebeck coefficient correspond to twice the standard deviations of measurements along four lines at each distance

profile in Fig. 2a, b corresponds this start of crystallization. The intermediate phase region beginning next to the PbTe base region appears single phase by SEM observation with backscattered electron mode. The formation of the single phase next to the PbTe base region is consistent with the phase diagrams which indicate peritectic reactions [15, 16, 18] but not with the one which shows a eutectic reaction between PbTe and $PbBi_4Te_7$ [17]. According to reported phase diagrams, the intermediate compound could be "$Pb_3Bi_4Te_9$" [15] or "$PbBi_2Te_4$" [16, 22]. The composition of the intermediate phase observed in the unidirectionally solidified sample by WDS in this work is located between "$PbBi_2Te_4$" and "$Pb_2Bi_6Te_{11}$ [22]" compositions. The maximum c_{Bi} in the PbTe phase corresponds to the maximum solubility in the PbTe phase at the peritectic temperature (583 °C [16]).

As indicated in Fig. 2b, Widmanstätten precipitates were observed in the PbTe solid solution base region which contains ~8 at.% Bi or more. The microstructure is shown Fig. 3a. The precipitates are too thin for explicit examination by WDS methods. It is likely that the precipitation occurs due to the decrease in the composition range of PbTe phase with decrease in temperature, which is discussed for more details in the next section.

Existence range of PbTe phase in the pseudo-binary PbTe–Bi_2Te_3 system

The formation of Widmanstätten precipitates in the unidirectionally solidified sample is thought to be caused by the decrease in solubility in the PbTe solid solution region during cooling. To confirm this, the solubility in PbTe is determined using PbTe/Bi_2Te_3 diffusion couples. Figure 4 shows an example of concentration profiles of the diffusion couples (annealed at 450 °C for 24 days). In determination of the phase boundaries, the fitted concentration profiles were extrapolated to the phase boundary positions [20]. The phase boundary compositions at each temperature is plotted in Fig. 1. In the figure, the maximum solubility in PbTe and the composition of the phase next to PbTe in the sample unidirectionally solidified using the Bridgman method (Fig. 2) are also plotted at the peritectic temperature (583 °C [16]). The phase boundary compositions determined from diffusion couples annealed at the same temperature but for different periods are consistent with each other within error ranges. Therefore, the local equilibrium in the diffusion couples is assumed to be valid. The solubility range of PbTe thus determined decreases with decrease in temperature as expected in the previous section: 15.6 ± 0.9 (583 °C) to $6.2^{+2.1}_{-1.7}$ (450 °C) at.% Bi.

To confirm the solubility range determined by the diffusion couple technique, an isothermal annealing experiment was carried out at 8 at.% Bi ($Pb_{40}Bi_8Te_{52}$) at 450 °C for 38 h after homogenization. In the phase diagram, the point for 8 at.% Bi and 450 °C is located in the two phase region (PbTe solid solution plus an intermediate phase). Figure 3b and c shows the microstructure after homogenization and after annealing at 450 °C for 38 h. As expected from the solubility, Widmanstätten precipitates were formed after the heat treatment. A powder XRD experiment was carried out on this sample to examine the phases. Figure 5 shows the XRD profiles with the reference profiles for PbTe [23], $PbBi_2Te_4$ [24], $PbBi_4Te_7$ [25], and Bi_2Te_3 [26]. The peak positions are mostly consistent with PbTe except for shoulders of the peak at 39.5°. The angles for the shoulders are most consistent with those for $PbBi_2Te_4$ but the peaks for $PbBi_4Te_7$ are also very close. It is difficult to identify the phase of precipitates only from the XRD profiles since the intensity from the precipitate phase is weak and the peak positions of $PbBi_2Te_4$ and $PbBi_4Te_7$ are close to each other.

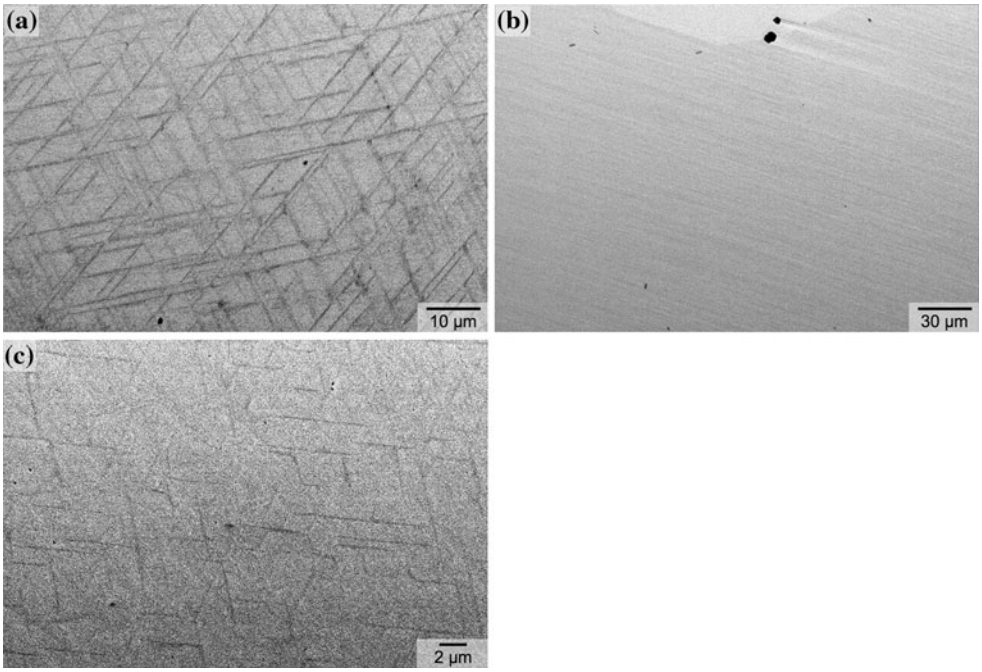

Fig. 3 Microstructure in the PbTe-rich region with Widmanstätten precipitates in $Pb_{14}Bi_{28.8}Te_{57.2}$ unidirectionally solidified by Bridgman method (**a**) and in PbTe–8Bi after homogenization at 585 °C for 7 days (**b**) and after homogenization followed by anneal at 450 °C for 38 h (**c**)

Composition of the Widmanstätten precipitates

The crystal structure of the precipitate phase is not entirely conclusive from the XRD profile shown in Fig. 5 alone. As mentioned earlier, it is difficult to measure the chemical composition of the precipitates using WDS as they are too thin. In the pseudo-binary PbTe–Bi_2Te_3 system, several ternary intermediate phases such as $PbBi_8Te_{13}$ [22], $PbBi_6Te_{10}$ [22], $PbBi_4Te_7$ [16, 27], $Pb_2Bi_6Te_{11}$ [22, 25], and $PbBi_2Te_4$ [24] have been reported. Of these compounds, the chemical composition of $PbBi_2Te_4$ is the closest to PbTe. It is, therefore, likely that the precipitates are $PbBi_2Te_4$. In order to check the stability of the $PbBi_2Te_4$ phase, we prepared samples with the composition corresponding to $PbBi_2Te_4$ and carried out isothermal heat treatments. Figure 6 shows the XRD profiles from the samples annealed at 550 °C for 7 days and further annealed at 350 °C for 10 days after 550 °C annealing (the composition and temperature are indicated in Fig. 1). While the positions of many of the largest peaks for PbTe, $PbBi_2Te_4$, $PbBi_4Te_7$, and Bi_2Te_3 such as the one at 27.7° are close to each other, those of minor peaks are separated well enough to identify phases. The peak positions for both of the two samples are almost identical and consistent with the reference profiles of $PbBi_2Te_4$ and PbTe (small volume fraction). This suggests that $PbBi_2Te_4$ is the stable crystal structure and should be the phase next to PbTe in the pseudo-binary PbTe–Bi_2Te_3 system at 350 and 550 °C. It is expected from the existence of the PbTe phase that the composition of "$PbBi_2Te_4$" phase is slightly deviated to a composition with more Bi content than the nominal composition of $PbBi_2Te_4$.

The XRD profile for $Pb_{40}Bi_8Te_{52}$ annealed at 450 °C for 38 h was refined using the Rietveld method ($R_p = 5.3\%$, $R_{wp} = 7.3\%$) as shown Fig. 5. The lattice parameter of PbTe solid solution (~6.2 at.% Bi) obtained in the analysis is 6.439 nm. This is slightly smaller than 6.454 nm [23] for PbTe without a tertiary element. The lattice parameter decreases since Bi^{3+} (ionic radius: 0.103 nm [28]), which has a smaller radius than Pb^{2+} (ionic radius: 0.119 nm [28]), substitutes for Pb^{2+} in the PbTe structure. It is also likely that the increase in the Bi content in the PbTe phase in the pseudobinary PbTe–Bi_2Te_3 system is accompanied with the formation of vacancies and causes an inward relaxation, which also contributes to the decrease in the lattice parameter. The Rietveld analysis indicated a 6.5% volume fraction of the secondary phase, which was assumed to be $PbBi_2Te_4$ in the analysis. Using the solubility of Bi in PbTe in the pseudo-binary PbTe–Bi_2Te_3 determined by the diffusion couple experiment, ~6.2 at.% Bi at 450 °C, the volume fraction of the secondary phase at 8 at.% Bi is estimated by a lever rule to be 7.9% for $PbBi_2Te_4$. Considering the errors in the Rietveld refinement, the agreement between the volume fractions of precipitates estimated by the Rietveld refinement (~6.2%) and lever rule (7.9%), is good. Karpinskii et al. [22] reported that $Pb_2Bi_6Te_{11}$ is formed at low temperatures due to the peritectoid reaction between $PbBi_2Te_4$ and $PbBi_4Te_7$.

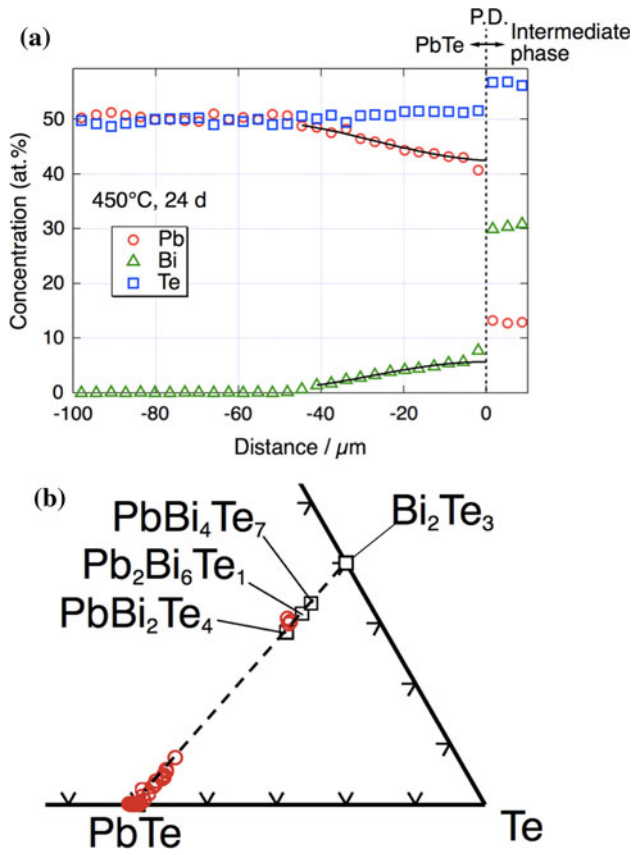

Fig. 4 An example of partial concentration profile for the PbTe phase base region in the vicinity of the interface between PbTe and an intermediate phase in a $PbTe/Bi_2Te_3$ diffusion couple annealed at 450 °C for 24 days. The concentrations are plotted as functions of distance in (**a**) and in the partial ternary phase diagram for the Pb–Te–Bi system (**b**)

However, the detailed crystal structure has not been clarified yet. Nevertheless, there is still a possibility that the precipitates have composition close to $Pb_2Bi_6Te_{11}$ even if the XRD pattern matches $PbBi_2Te_4$ (as found in Pb-Sb–Te phases). Assuming the precipitates to have composition $Pb_2Bi_6Te_{11}$, the lever rule gives 6.9% volume fraction for precipitates, which also agrees slightly better with the Rietveld refinement. On the other hand, the composition of the phase which appears next to the PbTe solid solution region in the diffusion couple (Figs. 1, 4) is located between the theoretical compositions of $PbBi_2Te_4$ and $Pb_2Bi_6Te_{11}$. It is likely that the phase of Widmanstätten precipitates is the same as the ternary intermediate phase formed next to PbTe in the diffusion couple and is also the same as the ternary phase formed next to the PbTe base region in the unidirectional solidification (the ternary phase shown in Fig. 2). To identify the precipitate phase, further studies on crystal structure, composition, and phase stability of "$Pb_2Bi_6Te_{11}$" phase are desired.

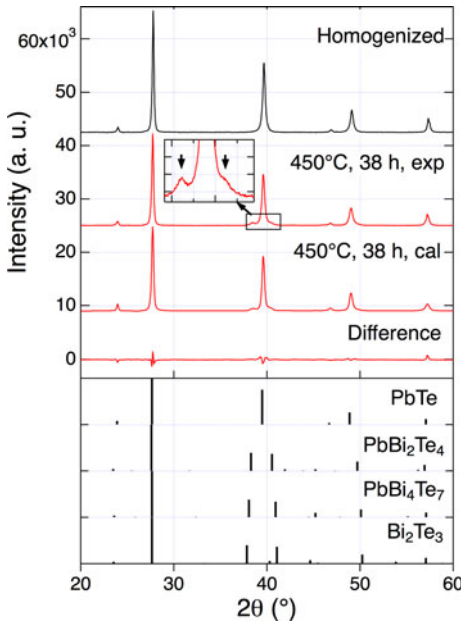

Fig. 5 XRD profiles for $Pb_{40}Bi_8Te_{52}$ after homogenization (585 °C, 7 days) and after anneal at 450 °C for 38 h. The small shoulders around 40° after anneal at 450 °C for 38 h indicated by *arrows* are from precipitate phase. The profile after anneal at 450 °C for 38 h was analyzed by Rietveld refinement ($R_p = 5.3\%$, $R_{wp} = 7.3\%$). The calculated profile and the difference between the experimental and calculated profiles are also shown. The reference profiles are shown below

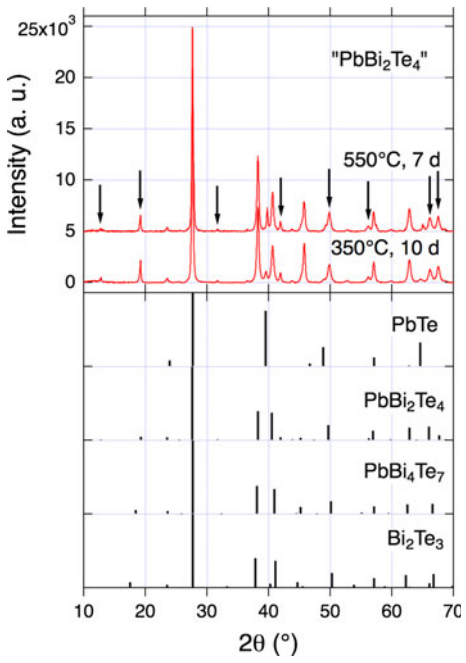

Fig. 6 XRD profiles for $Pb_{14.3}Bi_{28.6}Te_{57.1}$ (="$PbBi_2Te_4$") after anneal at 550 °C for 7 days and further anneal at 350 °C for 10 days. The reference profiles are shown below. *Arrows* show the minor peaks whose angles are consistent with $PbBi_2Te_4$

In the PbTe–Sb_2Te_3 system, $PbSb_2Te_4$ is the only ternary phase formed in the pseudo-binary system (but because of anti-site defects on the metal sites the ternary compound has actual chemical composition close to "$Pb_2Sb_6Te_{11}$" [29]). It is stable only in the small temperature window (576–587 °C) [10], and the precipitates formed in PbTe is not a ternary phase but Sb_2Te_3. In contrast, the precipitates formed in PbTe in this study are of a ternary phase in the PbTe–Bi_2Te_3 system. It is also interesting to note that Sb_2Te_3 precipitates via metastable $(Ag,Sb)_3Te_4$ phase, which takes a structure with a 7-layer stacking sequence, in $AgSbTe_2$ [30]. In PbTe–Bi_2Te_3 system, $PbBi_2Te_4$ possesses a 7-layer stacking sequence.

Orientation relationship between matrix PbTe and precipitates

Figure 7 shows the orientation relationship between the matrix PbTe and the precipitates obtained by EBSD analysis. In the analysis, crystal structure data for PbTe (NaCl-type structure (cubic), space group $Fm\,\bar{3}m$) [23] and $PbBi_2Te_4$ (rhombohedral structure, space group $R\bar{3}m$) [22, 24] were used. As discussed in the previous section, there is a possibility that the precipitates are $Pb_2Bi_6Te_{11}$, or even other related $(PbTe)_n(Bi_2Te_3)_m$ layered structures. However, even if it is the case, the orientation relationship examined here is not affected since the crystal structures of $PbBi_2Te_4$ and other likely ternary phases are similar to each other (all with rhombohedral structures) and also have similar lattice parameters (e.g. $a = 0.44356$ nm [22] and 0.4419 nm [22] for $PbBi_2Te_4$ and $Pb_2Bi_6Te_{11}$, respectively). The spots for (0001) plane for $PbBi_2Te_4$ and {111} for PbTe, and those for $<11\bar{2}0>$ for $PbBi_2Te_4$ and <110> for PbTe are located almost at the same position in the pole figures (Fig. 7c–f), respectively. Therefore, we conclude that the orientation relationship between the matrix PbTe and precipitates is $(0001)_{PbBi2Te4}//\{111\}_{PbTe}$, $<11\bar{2}0>_{PbBi2Te4}//<110>_{PbTe}$. The crystal structures and atomic configurations on {111} planes and (0001) plane of PbTe and $PbBi_2Te_4$, respectively, are shown in Fig. 8. Also, the normal vectors of precipitates in Fig. 7b are close to the normal vectors of the {111} family in PbTe. This means that the habit planes of the precipitation are {111} family in PbTe. This orientation relationship is exactly the same as what we have observed for the PbTe matrix–Sb_2Te_3 precipitates [9] and the $AgSbTe_2$ matrix–Sb_2Te_3 precipitates combinations [31], where precipitate Sb_2Te_3 takes a rhombohedral structure with the same space group $R\bar{3}m$ as the ternary intermediate phase in the present system takes. Based on the lattice parameter of PbTe containing Bi at the solubility range at 450 °C obtained by Rietveld refinement ($a = 6.439$ nm), the interatomic distance on {111} planes is 0.4553 nm. Assuming the

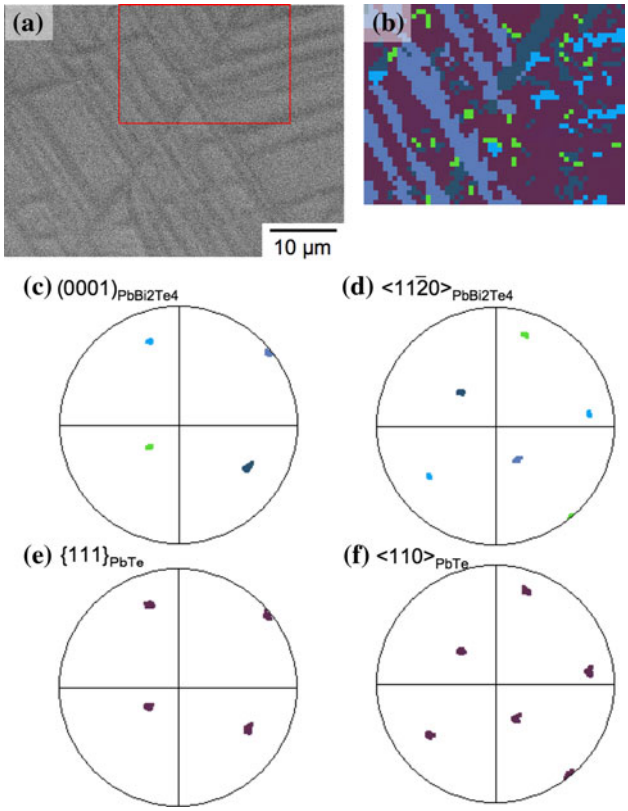

Fig. 7 EBSD analysis results for the PbTe-rich region with Widmanstätten precipitates in $Pb_{14}Bi_{28.8}Te_{57.2}$ unidirectionally solidified by Bridgman method. The area indicated by the *box* in the SEM (backscatter electron mode) image (**a**) was mapped in (**b**). Each point in (**b**) corresponds to the point that has the same color (or brightness) in pole figures (**c**–**f**). The pole figures are for (0001) plane (**c**) and $<11\bar{2}0>$ directions (**d**) in $PbBi_2Te_4$ and {111} planes (**e**) and <110> directions (**f**) in PbTe, respectively

precipitates are of $PbBi_2Te_4$, where the interatomic distance on (0001) plane is 0.44356 nm [22], this gives an ~3% lattice mismatch at the interface between the matrix PbTe and the precipitates, which is slightly smaller than in the case for PbTe–Sb_2Te_3 interface (~6.2%). This suggests that the interfaces could be semicoherent with misfit dislocations as were observed in PbTe–Sb_2Te_3 system [32] but with longer periods because of a smaller lattice mismatch.

Thermoelectric properties

Seebeck coefficient measured as a function of position in the sample is shown in Fig. 2c. In the region of PbTe with Widmanstätten precipitates, the Seebeck coefficient stays at a nearly constant $-46 \pm 2\ \mu VK^{-1}$ and transitioned to the intermediate phase region discontinuously because of the existence of the sharp interface between the PbTe base region and the intermediate phase. The spatial resolution of the scanning Seebeck measurement, on the order of 0.1 mm, is much coarser than the microstructure composed

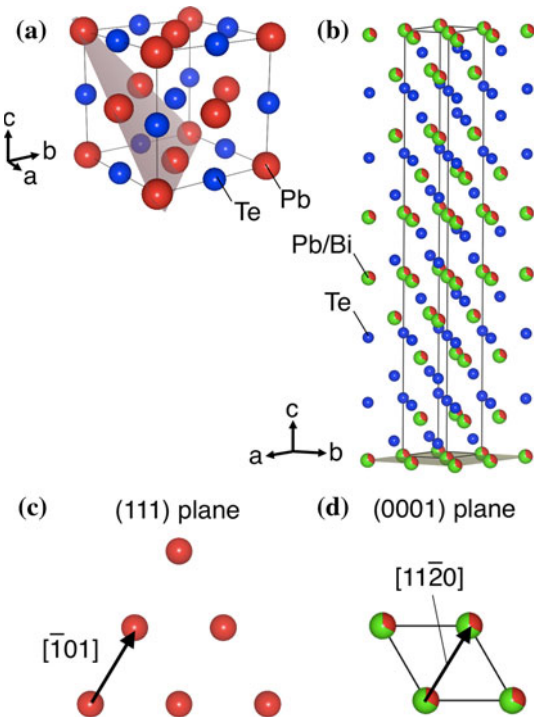

Fig. 8 Crystal structures of PbTe (**a**) and $PbBi_2Te_4$ (**b**) [24]. The EBSD results show that these two crystals have the orientation relationship $\{111\}_{PbTe}//(0001)_{Precipitate}$ and $<110>_{PbTe}//<11\bar{2}0>_{Precipitate}$. **c** and **d** shows a (111) plane of PbTe and (0001) plane of $PbBi_2Te_4$, respectively, which are indicated by *gray* in **a** and **b**

of fine Widmanstätten precipitates. In the composition range examined previously, the PbTe solid solution shows a peak in Seebeck coefficient ($-167\ \mu VK^{-1}$) at ~ 0.3 at.% Bi [14] and then the absolute value decreases monotonically to $-30\ \mu VK^{-1}$ at 1.94 at.% Bi [13, 14] or $-60\ \mu VK^{-1}$ at 0.84 at.% Bi [14]. In principle, each Bi subtstituted for a Pb should result on one free electron (n-type Seebeck expected) [33] but other defects may also be present. From the fact that precipitates are not observed in the bottom part of the PbTe phase (~ 6.5 at.% Bi), this region must be supersaturated with Bi_2Te_3 showing only PbTe solid solution phase. The Seebeck coefficient measured in this work indicates higher Bi concentration in PbTe than the previous studies. The optimal composition for the highest zT is ~ 0.3 at.% Bi [14]. To improve the thermoelectric zT, reduction of carrier concentration would also be essential. This could be done by doping with another element with $+1$ valence to compensate the high electron concentration.

Fine microstructure with coherent or semicoherent interfaces in the precipitation structure could result in significant lattice thermal conductivity reduction due to enhanced scattering of phonons by the difference in masses between the precipitates and the matrix [34, 35] or bond stiffness [34]. The atomic mass of Bi (208.98 u) is close to that of Pb (207.19 u) while Sb (121.76 u) is smaller. Therefore, the mass contrast between precipitates and matrix PbTe is not as significant in the present system PbTe–Bi_2Te_3 as in PbTe–Sb_2Te_3 [9]. Measurements of lattice thermal conductivities of both these systems will be a good reference regarding the role of mass contrast in thermal conductivity reduction and are underway. It should also be noted that the interfacial area per volume, which could be one of critical quantities which affect lattice thermal conductivity [1, 36], of Widmanstätten precipitates can be controlled through cooling rates, composition, or heat treatment temperature on the basis of phase transformation theories [10, 11].

Conclusion

Widmanstätten precipitates are formed in a PbTe base compound in unidirectional solidification using the Bridgman method with a $Pb_{14}Bi_{28.8}Te_{57.2}$ composition, which lies on the pseudo-binary line in the PbTe–Bi_2Te_3 system. The formation of precipitates is caused by the decrease in the composition range of PbTe phase with decrease in temperature, which has been confirmed by the compositional variation in the unidirectionally solidified sample and experiments using diffusion couples: 15.6 ± 0.9 (583 °C) to $6.2^{+2.1}_{-1.7}$ (450 °C) at.% Bi. Widmanstätten precipitates are also formed by an isothermal heat treatment of the $Pb_{40}Bi_8Te_{52}$ composition at 450 °C. The precipitates are of a ternary phase such as $PbBi_2Te_4$ but may have actual composition closer to $Pb_2Bi_6Te_{11}$. The precipitation occurs on {111} habit planes in PbTe with orientation relationship $(0001)_{precipitate}//\{111\}_{PbTe}$ and $<11\bar{2}0>_{precipitate}//<110>_{PbTe}$. The size scale should be controllable on the basis of phase transformation theories as has been done for the PbTe–Sb_2Te_3 system. The Seebeck coefficient of PbTe with Widmanstätten precipitates is $-46 \pm 2\ \mu VK^{-1}$. To improve the power factor for thermoelectric applications, the carrier concentration needs to be reduced.

Acknowledgements We would like to thank Nathan Marolf for help in sample preparations. This work was funded by the PRESTO program (PRESTO: Precursory Research for Embryonic Science and Technology) of Japan Science and Technology Agency and ARO-MURI. M.B.T was supported by MURF program at California Institute of Technology. Microscopy facilities are supported by NSF CSEM MRSEC at Caltech.

References

1. Dresselhaus MS, Chen G, Tang MY, Yang R, Lee H, Wang D, Ren Z, Fleurial J-P, Gogna P (2007) Adv Mater 19:1043
2. Medlin DL, Snyder GJ (2009) Curr Opin Colloid Interface Sci 14:226
3. Kanatzidis MG (2010) Chem Mater 22:648

4. Pei Y, Lensch-Falk J, Toberer ES, Medlin DL, Snyder GJ (2011) Adv Funct Mater 21:241
5. Snyder GJ, Toberer ES (2008) Nat Mater 7:105
6. Ikeda T, Collins LA, Ravi VA, Gascoin FS, Haile SM, Snyder GJ (2007) Chem Mater 19:763
7. Ikeda T, Ravi VA, Collins LA, Haile SM, Snyder GJ (2007) J Electron Mater 36:716
8. Yang F, Ikeda T, Snyder GJ, Dames C (2010) J Appl Phys 108:034310
9. Ikeda T, Ravi VA, Snyder GJ (2009) Acta Mater 57:666
10. Ikeda T, Snyder GJ (2010) Mater Res Soc Symp Proc 1267:DD06
11. Ikeda T, Marolf NJ, Bergum K, Toussaint MB, Heinz NA, Ravi VA, Snyder GJ (2011) Acta Mater. doi:10.1016/j.actamat.2011.01.006
12. Dames C, Chen G (2005) In: Rowe DM (ed) Thermoelectircs handbook: macro to nano. CRC Press, Boca raton
13. Christakudi TA, Christakudis GC, Borissova LD (1995) Phys Status Solidi 190B:537
14. Zhu P, Imai Y, Isoda Y, Shinohara Y, Jia X, Zoub G (2006) J Alloys Compd 420:233
15. Hirai T, Takeda Y, Kurata K (1967) J Less Common Met 13:352
16. Chami R, Brun G, Tédenac J-C, Maurin M (1983) Rev Chim Miner 20:305
17. Golovanova NS, Zlomanov VP, Tananaeva OI (1983) Inorg Mater 19:669
18. Shelimova LE, Karpinskii OG, Konstantinov PP, Avilov ES, Kretova MA, Zemskov VS (2006) Bi-Pb-Te Phase Diagram, ASM Alloy Phase Diagrams Center, P. Villars, editor-in-chief; H. Okamoto and K. Cenzual, section editors; http://www1.asminternational.org/AsmEnterprise/APD, ASM International, Materials Park, OH
19. Flewitt PEJ, Wild RK (1994) Physical methods for materials characterization. Institute of Physics Publishing, Bristol and Philadelphia
20. Bergum K, Ikeda T, Snyder GJ (2011) In preparation
21. Chen N, Gascoin F, Snyder GJ, Müller E, Karpinski G, Stiewe C (2005) Appl Phys Lett 87:171903
22. Karpinskii OG, Shelimova LE, Avilov ES, Kretova MA, Zemskov VS (2002) Inorg Mater 38:17
23. Noda Y, Masumoto K, Ohba S, Saito Y, Toriumi K, Iwata Y, Shibuya I (1987) Acta Crystallogr 43C:1443
24. Zhukowa TB, Zaslavskii AI (1971) Sov Phys Crystallogr 16:796
25. Shelimova LE, Karpinskii OG, Svechnikova TE, Avilov ES, Kretova MA, Zemskov VS (2004) Inorg Mater 40:1264
26. Feutelais Y, Legendre B, Rodier N, Agafonov V (1993) Mater Res Bull 28:591
27. Shelimova LE, Karpinskii OG, Konstantinov PP, Avilov ES, Kretova MA, Zemskov VS (2004) Inorg Mater 40:451
28. Shannon RD (1976) Acta Crystallogr 32A:751
29. Ikeda T, Toberer ES, Ravi VA, Snyder GJ, Aoyagi S, Nishibori E, Sakata M (2009) Scripta Mater 60:321
30. Sugar JD, Medlin DL (2010) J Mater Sci. doi:10.1007/s10853-010-4984-4
31. Medlin DL, Sugar JD (2010) Scripta Mater 62:379
32. Heinz NA, Ikeda T, Snyder GJ, Medlin DL (2011) In preparation
33. Toberer ES, May AF, Snyder GJ (2010) Chem Mater 22:624
34. Kim W, Zide J, Gossard A, Klenov D, Stemmer S, Shakouri A, Majumdar A (2006) Phys Rev Lett 96:045901
35. Sootsman JR, Pcionek RJ, Kong H, Uher C, Kanatzidis MG (2006) Chem Mater 18:4993
36. Jeng M-S, Yang R, Song D, Chen G (2008) J Heat Transf 130:042410